

# Optical Controllable Spin-Polarization in Two Dimensional Altermagnets via Robust Spin-Momentum Locking Excitons

Jiuyu Sun, Jinzhe Han, Yongping Du,<sup>\*</sup> and Erjun Kan<sup>†</sup>  
 MIT Key Laboratory of Semiconductor Microstructure and Quantum Sensing,  
 Nanjing University of Science and Technology, Nanjing 210094, China  
 (Dated: June 13, 2025)

Spin-momentum locking (SML) excitons in two-dimensional semiconductors are appealing to programmable optical control of spin-polarized carriers in ultrafast spintronics. To address the current thirst for long-lived excitons with zero-external-field stability and room-temperature spin-polarization, we hereby predict the existence of intrinsically SML excitons in altermagnetic  $V_2X_2O$  ( $X = S, Se$ ) driven by giant non-relativistic spin-splittings ( $> 1.2$  eV). First-principles calculations reveal SML excitons with binding energies exceeding 1400 meV in monolayers and 430 meV in their van der Waals heterobilayers, along with stacking-dependent optical selection rules for tunable interlayer excitons. These remarkable physical properties, combined with their long radiative lifetimes, strongly suggest the feasibility of SML excitons with robust spin-polarization at room temperature. Our work provides a new paradigm for SML exciton physics via the novel altermagnetism, opening up new possibilities for all-optical manipulation in advanced opto-spintronics.

## I. INTRODUCTION

The optical control of spin-polarized carriers in two-dimensional (2D) semiconductors has emerged as a pivotal area of research, offering ultrafast manipulation of spin and charge and non-contact operation through circularly polarized light[1–4]. Recently, spin-momentum locking (SML) excitons in 2D semiconductors attract considerable attention, which are bound electron-hole pairs with spin orientation intrinsically tied to crystal momentum[5–9]. SML excitons, in principle, bypass the need for external magnetic fields by leveraging momentum-dependent spin textures, offering deterministic optical addressability, extended spin lifetimes, and robust quantum coherence, which are critical for advancing energy-efficient spin logic and room-temperature quantum technologies.

Although remarkable progresses have been made via an intensive pursuit of SML excitons, significant challenges remain in their practical implementation. In conventional non-magnetic 2D materials like transition metal dichalcogenides (TMDCs), e.g.  $MoS_2$ , the generation of SML excitons via circularly polarized light relies on the spin-orbit coupling (SOC) induced spin-splitting[9–12]. However, the spin-splitting is inherently weak, on the order of tens of meV, unless toxic heavy elements are used[13–15]. The consequent difficulty for spin-selective identification and manipulation, as well as the rapidly decay of spin-polarization at room temperature, require cryogenic temperatures or external stimuli for stabilization[16–22]. These challenges expose the fundamental limits of relativistic mechanisms in achieving robust spin polarization in non-magnetic 2D semiconductors.

Efforts to overcome these issues have turned to the recently discovered 2D magnetic semiconductors[23–27], which host long-lived spin-polarized excitons due to their intrinsic long-range magnetic orders. For instance, spin-polarized excitons are reported in chromium trichlorides (ferromagnetic) and transition metal phosphorous trichalcogenides (antiferromagnetic), with large binding energies in theory[28–32] and clear spin-polarized optical responses in experiment[33, 34]. Yet, challenges persist: the ferromagnetism only supports spin-polarized states in the spin-majority direction and can hardly survive in 2D semiconductors at room temperature; the lack intrinsic spin-splitting in antiferromagnets makes it difficult to achieve efficient optical control of spin-polarized excitons without additional symmetry-breaking operations. These trade-offs underscore a critical demand for a material platform that intrinsically combines considerable non-relativistic spin-splitting, room-temperature stability, and efficient optical control.

In this work, exemplified by the prototypical  $V_2X_2O$  ( $X = S, Se$ ) systems, we propose that novel 2D altermagnetic semiconductors[35–39], present a promising material platform to satisfy this demand. These materials uniquely combine thermal stability as antiferromagnets—zero net magnetization and ferromagnetic-like non-relativistic spin-splittings[35, 40–44]. As illustrated in Figure 1(a), their symmetry-protection induced momentum-dependent spin textures in both valence and conduction bands[35, 36, 39, 45, 46] enable the generation and manipulation of SML excitons via circular polarized light. As a prime example, first-principles calculations reveal that  $V_2X_2O$  systems host intrinsically SML excitons with binding energies exceeding 1400 meV in monolayers and 430 meV in their van der Waals heterobilayer (vdWH), as well as stacking-dependent optical selection rules for tunable interlayer SML excitons. More importantly, the giant non-relativistic spin-splittings, exceeding 1.2 eV in  $V_2X_2O$ , could drastically reduce the spin-valley depolarization of the SML excitons via various rou-

<sup>\*</sup> njustdyp@njust.edu.cn

<sup>†</sup> ekan@njust.edu.cn

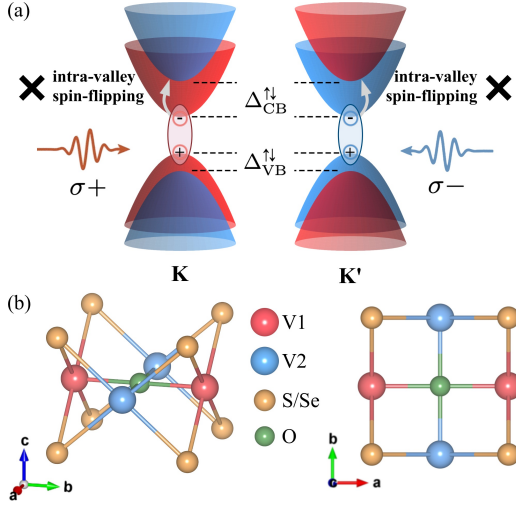


FIG. 1. Schematic diagram of the generation of SML excitons at  $K$  and  $K'$  valleys, where the large exchange-induced spin-splittings for both valence and conduction bands ( $\Delta_{VB}^{\uparrow\downarrow}$  and  $\Delta_{CB}^{\uparrow\downarrow}$ ) would remarkably reduce the intra-valley spin-flipping, e.g. for conduction bands. (b) Atomic structure of monolayer  $V_2X_2O$  with V1 (spin-up V), V2 (spin-down V), S/Se, O atoms colored in red, blue, orange and green, respectively.

tines, e.g. intra-valley spin-flipping in Figure 1(a). This altermagnetic mechanism transcends the limitations of SOC-driven systems and conventional magnets, enabling spin logic operations without cryogenic or external-field constraints.

## II. COMPUTATIONAL METHODS

Our density functional theory calculations were performed using the Quantum Espresso package[47] with the optimized norm-conserving Vanderbilt pseudopotentials[48, 49]. All geometric structures were fully relaxed with the PBE[50] functional, and the lattice constant of unit cell of  $V_2Se_2O$  monolayer was optimized to be 3.88 Å, which is in agreement with previous works[35, 36, 51]. The Néel temperatures of the monolayers are estimated[52] to be over 700 K. For the quasiparticle band structures, we adopted the band structures and wavefunctions by PBE+ $U$  with  $U_{\text{eff}} = 4.5$  eV, after a comprehensive evaluation of various methods[53–55] (see Supplemental Materials (SM)[56]). The optical response (dielectric function) and exciton energies are obtained by solving the Bethe-Salpeter equation (BSE) with a static dielectric screening. All the spin-resolved many-body perturbation calculations[57–61] were performed by using BerkeleyGW package[62, 63], and more computational details and convergence tests could be found in the SM[56]. Furthermore, the radiative lifetime of  $S$ -th exciton at temperature  $T$  (K) is estimated via approach

by Bernardi et al.[64, 65]:

$$\langle \tau^S \rangle(T) = \tau_0^S \frac{3}{4} \left\{ \frac{(E_{\text{ex}}^S)^2}{2M^S c^2} \right\}^{-1} k_B T, \quad (1)$$

with the

$$\tau_0^S = \frac{A_{\text{uc}} \hbar^2 c}{8\pi e^2 E_{\text{ex}}^S \mu_S^2}, \quad (2)$$

where  $A_{\text{uc}}$  is the area of the unit cell and  $E_{\text{ex}}^S$  is the excitation energy of the  $S$ -th zero momentum exciton with effective mass  $M^S$ .  $\mu_S^2$  is the square of the dipole matrix element of the  $S$ -th exciton obtained by solving BSE.

## III. RESULTS AND DISCUSSIONS

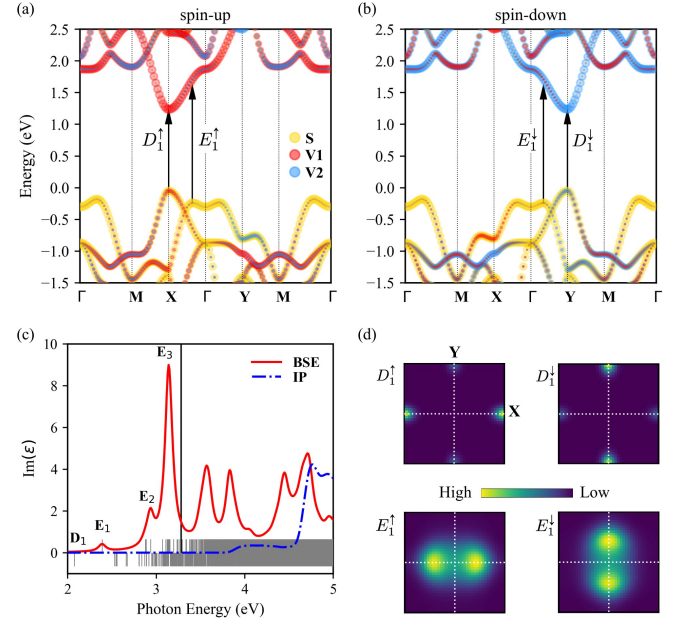


FIG. 2. Calculated results for the  $V_2S_2O$  monolayer. The (a) spin-up and (b) spin-down band structures by PBE+ $U$ , projected onto the V1, V2 and S atoms with the weights proportional to the radii of the colored circles. Energy zero is at the top of valence band. The vertical arrows indicate the transitions of corresponding excitons. (c) Optical spectra  $\text{Im}(\epsilon)$  by BSE and IP for the light polarization along  $[110]$ . The vertical grey ticks indicate the excitonic energies with module square of dipole moment larger and smaller than  $1 \times 10^{-2}$  are shown separately upon and below zero axis, respectively. The single-particle band gap after the rigid scissors operator is indicated by the black vertical line. (d) Reciprocal-space distributions of optical transitions for selected SML excitons.

As shown in Figure 1(b), the  $V_2X_2O$  monolayer has a square geometry with the collinear magnetic moments on the two V atoms aligning oppositely along the out-of-plane  $z$ -direction. We use  $V_2S_2O$  to illustrate the common electronic and optical properties for the monolayers,

and more results for  $\text{V}_2\text{Se}_2\text{O}$  are available in the SM[56]. The projected band structures for both spin channel are shown in Figure 2(a-b). Due to the spin group  $|C_2||C_{4z}|$ , the bands are spin degenerate along  $\Gamma$ - $M$ , whereas they are identical in energy but with opposite spin splittings along  $\Gamma$ - $X$  and  $\Gamma$ - $Y$ . There are two pairs of valleys around both the valence band maximum (VBM) and conduction band maximum (CBM) at  $X$  and  $Y$  points for spin-up and spin-down channels, respectively. The CBM valley at  $X$  ( $Y$ ) is almost 100% contributed by the  $d_{xz}$  ( $d_{yz}$ ) orbital of V1 (V2), while the VBM valleys exhibit a significantly hybrid nature, consisting of  $p$  and  $d$  orbitals from S and V atoms, respectively. We found that the band gap and the spin splitting for VBM ( $\Delta_{\text{VB}}^{\uparrow\downarrow}$ ) largely depend on the computational methodology[56]. A direct band gap of 1.28 eV is obtained with  $U_{\text{eff}} = 4.5$  eV. On the contrary, the spin splitting at CBM valleys ( $\Delta_{\text{CB}}^{\uparrow\downarrow}$ ) is not much affected by the computational methods and retains a large  $\Delta_{\text{CB}}^{\uparrow\downarrow}$  over 1.1 eV, which is crucial for achieving robust spin-valley polarization. Overall, such a SML band structure with large spin splitting provides a robust foundation for generating the SML excitons in  $\text{V}_2\text{S}_2\text{O}$  sheets with circular-polarized light.

TABLE I. Direct band gaps ( $E_g$ ) by PBE+ $U$ , spin-splittings in valence and conduction bands ( $\Delta_{\text{VB}}^{\uparrow\downarrow}$  and  $\Delta_{\text{CB}}^{\uparrow\downarrow}$ ), the lowest bright excitonic energy ( $E_{\text{ex}}^1$ ) and the corresponding excitonic binding energy ( $E_b^1$ ) in monolayers and vdWHs in the unit of eV.

	$E_g$	$\Delta_{\text{VB}}^{\uparrow\downarrow}$	$\Delta_{\text{CB}}^{\uparrow\downarrow}$	$E_{\text{ex}}^1$	$E_b^1$
$\text{V}_2\text{S}_2\text{O}$	1.28	0.76	1.27	2.39	1.55
$\text{V}_2\text{Se}_2\text{O}$	0.86	1.23	1.34	2.55	1.40
AB	0.53	1.24	1.27	2.10	0.43
AB'	0.80	0.81	0.28	2.61	0.96

We then solved the BSE for the dielectric function and exciton energies, and plotted the calculated results in Figure 2(c). To account for quasiparticle self-energy correction (see detailed discussion in the SM[56]), we adopted a scissors operator of 2.0 eV to the bands by PBE+ $U$ , resulting in an enlarged band gap of 3.28 eV indicated by the vertical solid line in Figure 2(c). Comparing the optical spectra by BSE and independent-particle approximation (IP), we identify three main excitonic absorption peaks with significant optical responses below the shifted band gap and the absorption edge (around 3.8 eV) of the IP spectrum, indicating strong excitonic effects in the  $\text{V}_2\text{S}_2\text{O}$  monolayer. The highest absorption peak at about 3.1 eV corresponds to the  $E_3$  exciton, which is largely contributed by the transitions off the highly polarized lines ( $\Gamma$ - $X$  and  $\Gamma$ - $Y$ ). This implies a much weaker spin selectivity in momentum-space of  $E_3$ , which is not the SML excitons we focus on in this work.

In Figure 2(d), we plotted the reciprocal-space distributions of optical transitions for several representative SML excitons, namely the bright excitons ( $E_1^{\uparrow/\downarrow}$ ) and dark excitons ( $D_1^{\uparrow/\downarrow}$ ) of spin-up/spin-down.  $E_1^{\uparrow}$ , as well

as the spin counterpart  $E_1^{\downarrow}$ , is the lowest energy (2.39 eV) bright exciton. Compared to the  $A$ -excitons in TMDCs,  $E_1^{\uparrow}$  ( $E_1^{\downarrow}$ ) has a much larger binding energy of 1.55 eV and a longer radiative lifetime ( $\sim 100$  ps at 4K and  $\sim 7.32$  ns at 300K), implying a longer coherence time to recombine vertically. The optical transition distributions in Figure 2(d) confirm a clear momentum-selectivity for  $E_1^{\uparrow}$  and  $E_1^{\downarrow}$ , which couple to spin-up and spin-down channels, respectively. Interestingly,  $E_1^{\uparrow}$  ( $E_1^{\downarrow}$ ) is mainly contributed by the transitions from the saddle point of the VB near  $\Gamma$  to the hillside of the CB valley along  $\Gamma$ - $X$  ( $\Gamma$ - $Y$ ). In fact, the transitions from VBM to CBM are parity-forbidden, with VBM and CBM belonging to  $B_{2\mu}$  and  $A_{\mu}$  irreducible representations, respectively. Consequently, the corresponding excitons are found dark, i.e. spin-up polarized  $D_1^{\uparrow}$  and spin-down polarized  $D_1^{\downarrow}$ , whose reciprocal-space distributions of optical transitions are mainly around  $X$  and  $Y$ , respectively.

It is noteworthy that such an optical selection rule dominated by the spatial inversion symmetry, leading to dark SML excitons at valleys, represents one of the most significant differences between  $\text{V}_2\text{X}_2\text{O}$  and TMDC monolayers. On the other hand, these dark excitons could turn bright once the spatial inversion symmetry is broken. For instance, one can build a so-called Janus structure by substituting S atom in one of the two sublayers with a Se atom, or stack different monolayers into a heterobilayer, i.e. the  $\text{V}_2\text{S}_2\text{O}/\text{V}_2\text{Se}_2\text{O}$  vdWH.

In this work, we focus on the latter, for the sake of feasibility in experiment and promising advantages of forming interlayer excitons in vdWHs. We shall start with the most stable stacking order, i.e. AB-stacking in Figure 3(a). The projected band structure of AB-stacking in Figure 3(b) exhibits an obvious Type-II band alignment, and the VBM and CBM are from  $\text{V}_2\text{Se}_2\text{O}$  and  $\text{V}_2\text{S}_2\text{O}$  monolayers, respectively. In addition, the valleys of spin-up (spin-down) in the two monolayers are vertically aligned at  $X$  ( $Y$ ), meaning the VBM and CBM at each valley belong to the same spin-channel. The direct band gap, with the broken inversion symmetry, enables direct optical transition between VBM and CBM and therefore the formation of optically bright interlayer excitons at  $X$  ( $Y$ ) valleys.

In Figure 4(a) and (b), we plot the optical spectra of AB-stacking by BSE, as well as the eigenvalues for the excitons (see Figure 4(b) with details). In the following, we denote the intralayer and interlayer excitons as  $E_S^{\uparrow/\downarrow}@M$  and  $IX_S^{\uparrow/\downarrow}@M$  in a particular system  $M$  (e.g. AB for AB-stacking vdWH), respectively, where  $S$  is the index of excitons labeled in Figure 4(a-b) and  $\uparrow/\downarrow$  means spin direction of the exciton if needed. The two dominant absorption peaks at 2.8 and 3.4 eV are assigned to the  $E_1@AB$  and  $E_2@AB$ , which are both intralayer excitons. As shown by the real-space excitonic wavefunction modulus ( $|\psi(r_e, r_h)|^2$ ) in Figure 4(c), both the electron and hole of  $E_1@AB$  distribute in the  $\text{V}_2\text{Se}_2\text{O}$  layer. The reciprocal-space distribution of transitions along  $\Gamma$ - $X$  for

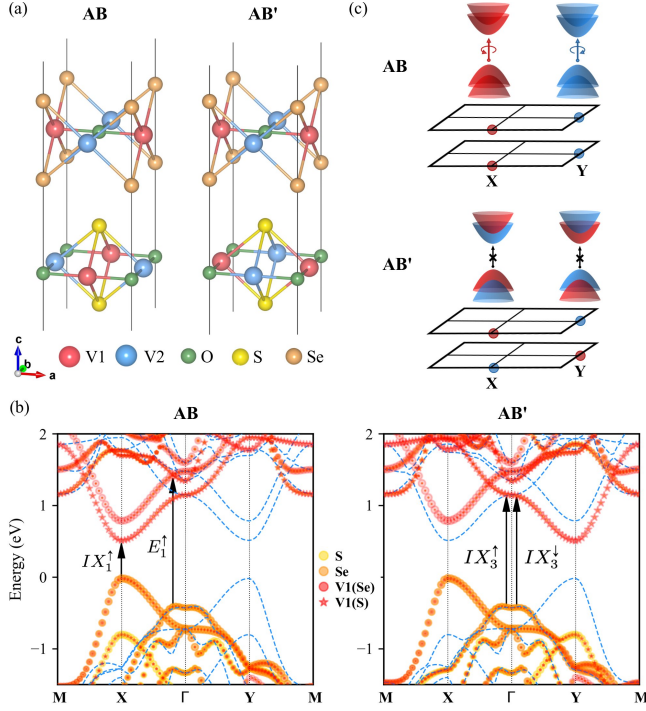


FIG. 3. The (a) geometry structures, (b) spin-resolved projected band structures by PBE+U and (c) demonstration of optical selection rules of the interlayer excitations for AB and AB' stacked vdWHs. For a clear presentation, only the spin-up bands are projected onto the V1, S and Se atoms, while the spin-down bands are plotted with blue dashed lines for reference. The V1(S) and V1(Se) stands for the V1 (spin-up) atoms in the  $V_2S_2O$  and  $V_2Se_2O$  layers, respectively. The vertical arrows indicate the transitions of corresponding excitons.

$E_1^\uparrow@AB$  reveals its SML nature similar to the  $E_1$  exciton in the  $V_2S_2O$  monolayer. The  $E_2@AB$  is in fact the non-SML  $E_3$  exciton in  $V_2S_2O$  monolayer (3.2 eV, see Figure 2)

The three peaks below  $E_1$  are all interlayer excitons in AB-stacking, namely,  $IX_1$ ,  $IX_2$  and  $IX_3$ . We only discuss  $IX_1$  here, since similar properties are found for  $IX_2$  and  $IX_3$  (see the SM[56]). Our calculations show the dipole oscillator strength of  $IX_1^\uparrow@AB$  is mostly (over 99%) contributed by the transitions between the VBM and CBM at X valley, indicating intrinsically perfect spin-valley polarization during excitation. The  $|\psi(r_e, r_h)|^2$  in Figure 4(c) clearly demonstrates its interlayer distribution, where the hole is fixed in the  $V_2Se_2O$  layer and the electron resides in the  $V_2S_2O$  layer. This confirms that optically active SML interlayer excitons can indeed be generated at the X(Y) valley in  $V_2S_2O/V_2Se_2O$  vdWH. Furthermore, the estimated binding energy of  $IX_1@AB$  is over 430 meV, which exceeds those in TMDC vdWHs by at least 25%. In addition, the  $\tau^{IX_1}(4K)$ ,  $\tau^{IX_1}(300K)$  in AB-stacking are estimated to be  $\sim 100$  ps and  $\sim 200$  ns, respectively, demonstrating that  $IX_1$  exhibits significantly longer lifetimes

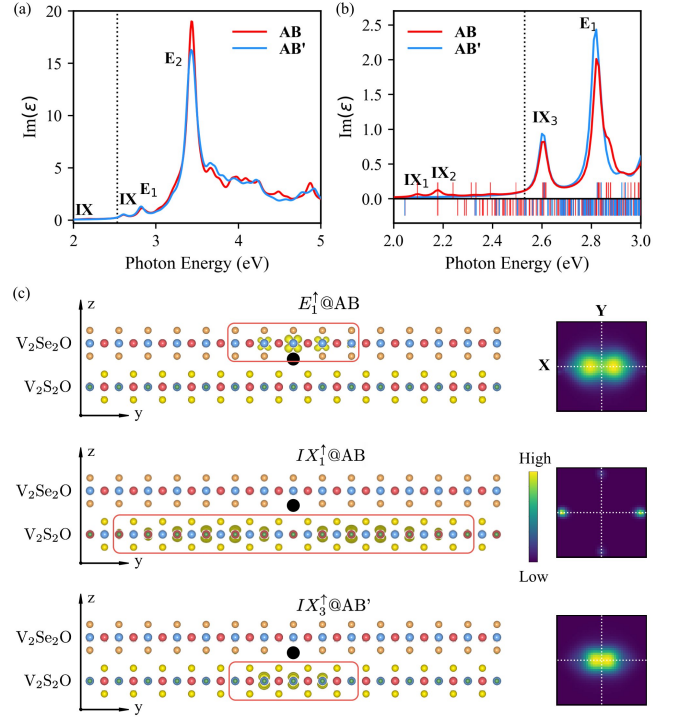


FIG. 4. (a) The optical spectra  $Im(\epsilon)$  with the light polarization along [110] for AB and AB' vdWHs, color coded with red and blue, respectively. The single-particle band gaps of the whole vdWH after a rigid 2.0 eV scissors operator are indicated by the vertical dotted lines. (b) The detailed optical spectra to show the low-lying excitons. The vertical ticks in red(blue) indicate the excitonic energies for AB(AB')-stacking, with module square of dipole moment larger and smaller than  $1 \times 10^{-2}$  are shown separately upon and below zero axis, respectively. (c) The real-space excitonic wavefunction and reciprocal-space distributions of optical transitions for the excitons  $E_1^\uparrow@AB$ ,  $IX_1^\uparrow@AB$  and  $IX_3^\uparrow@AB'$  in spin-up channel.

than the interlayer excitons in TMDC vdWHs at both low and room temperatures.

Recently, the introduction of a rotational misalignment between the two layers in vdWHs offers a fascinating modulation of the interlayer excitons via the formation of local stacking-order dependent moiré potential[8, 11, 12], establishing a new field termed *twistronics*. In this context, we consider another stacking order, i.e. AB'-stacking in Figure 3(a), which could be obtained by rotating one of the layers in AB-stacking by  $90^\circ$  with a total energy increase of 10 meV per unit cell. Apart from their spin configurations, AB- and AB'-stackings have the same geometry. Therefore, the two calculated band structures in Figure 3(b) are almost identical in energy. However, the spin lattices (V atoms) of AB- and AB'-stackings exhibit antiferromagnetic and ferromagnetic alignments along the c-axis, respectively, leading to qualitatively different spin-dependent band structures. In AB'-stacking, the  $90^\circ$  rotation switches the X and Y in the original Brillouin zone of the operated mono-

layer ( $V_2S_2O$  here). As a result, the spin-valleys in the two monolayer are anti-aligned, meaning the VBM and CBM at each valley in AB'-stacking reside in opposite spin channels.

Consequently, such an anti-aligned SML configuration in AB'-stacking leads to the forbidden interlayer transitions at  $X(Y)$  valleys due to the spin-flipping. As demonstrated by the optical selection rules in Figure 3(c), bright interlayer excitons ( $IX$ s) at  $X(Y)$  could be selectively generated by circularly polarized light exclusively in AB-stacking, while those in AB'-stacking are dark in principle. As expected, although Figure 4(a) shows roughly identical optical spectra of the two stackings, the main disparity between the spectra comes with the interlayer excitonic peaks in Figure 4(b). The spectrum of AB'-stacking exhibits no interlayer excitonic peaks below the intralayer  $E_1@AB'$ , except an  $IX_3@AB'$ . Given the clear interlayer distributed  $|\psi(r_e, r_h)|^2$ , one may be surprised how this  $IX_3@AB'$  survives under the spin-flip restriction. In fact,  $IX_3^\uparrow@AB'$  are mostly generated by the optical transitions around  $\Gamma$  point with a slight dispersion along  $\Gamma$ - $X$  (see Figure 3 and 4), highlighting the distinct nature of  $IX_3^\uparrow@AB'$  against  $IX_3@AB$  at  $X(Y)$  valleys. This  $IX_3^\uparrow@AB'$  cannot be regarded as SML excitons, since  $IX_3^\uparrow@AB'$  and its counterpart  $IX_3^\downarrow@AB'$  are too close to distinguish in the momentum-space. Therefore, only  $IX_1$ ,  $IX_2$  and  $IX_3$  in AB-stacking are the expected SML interlayer excitons with robust spin-valley coupling, indicating an effective tunability of the SML excitons upon the stacking order and a potential application in the twistrionics.

Lastly, we discuss the possible spin dynamics and address the improvement of spin-polarization in  $V_2X_2O$  as proposed above. We take the lowest-energy interlayer excitons in AB-stacking ( $IX_1@AB$ ) for example, due to the robust spin-valley coupling and spatial separation induced long lifetime. Mediated by exchange-interaction, SOC or phonons, there are several possible relaxation routines for  $IX_1$  that lead to spin-valley depolarization, which could be simply classified into intra-valley and inter-valley spin-relaxations[16–20, 22]. For the former, either or both carriers could vertically hop to the higher states of opposite spin, which cause the single or double (exchange) spin-flippings. According to Fermi's Golden Rule, the probabilities of transitions are, in principle, proportional to  $1/\Delta_{CB}^{\uparrow\downarrow}$  ( $1/\Delta_{VB}^{\uparrow\downarrow}$ ) or  $1/(\Delta_{CB}^{\uparrow\downarrow}\Delta_{VB}^{\uparrow\downarrow})$  for the single or double spin-flippings, respectively. The giant non-relativistic  $\Delta_{VB}^{\uparrow\downarrow}$  and  $\Delta_{CB}^{\uparrow\downarrow}$  over 1.2 eV for AB-stacking (see Table I) significantly suppress the intra-valley relaxation, no matter which mechanism takes place. The same principle applies for the inter-valley scattering processes with spin conservation, e.g., a

spin-up excited electron further hopping from VBM@ $X$  to a higher state of spin-up at  $Y$  valley. On the contrary, the SOC-induced splittings in TMDCs are down to tens of meV—the energy magnitude of room-temperature thermal fluctuation, which is a much smaller energy barrier to overcome. The other inter-valley scattering with spin flipped usually requires a collaboration of strong SOC and electron-phonon coupling[14, 21, 22], which could be further suppressed in  $V_2X_2O$  systems thanks to their weak SOC. Therefore, we expect a room-temperature robust spin-valley polarization for  $IX_1@AB$ , which indeed requires direct confirmation through non-adiabatic dynamical simulations or experiments in the future. Overall, we suggest that SML excitons with long-standing spin-polarization could widely exist in 2D altermagnetic semiconductors, provided with similar SML band structures and large spin-splittings.

#### IV. CONCLUSIONS

In summary, our first-principles calculations predict intrinsically SML excitons in 2D altermagnetic  $V_2X_2O$  with large excitonic binding energies over 1400 meV in monolayers and 430 meV in vdWH, giant non-relativistic spin-splitting over 1.2 eV. This altermagnetic mechanism locks spin orientation to momentum without SOC, enabling room-temperature-stable spin-polarization. Stacking-dependent symmetry breaking in vdWH further allows tunable bright/dark interlayer excitons. These results establish 2D altermagnets as a novel platform for ultrafast opto-spintronics, offering deterministic spin manipulation and enhanced quantum coherence for advanced device applications.

#### ACKNOWLEDGMENTS

This work was financially supported by the Ministry of Science and Technology of the People's Republic of China (No.2022YFA1402901), the National Natural Science Foundation of China (NSFC No.T2125004, No.U24A2010, No.12274228 and No.22303041), the NSF of Jiangsu Province (No.BK20230908), Fundamental Research Funds for the Central Universities (No.30922010102, No.30922010805 and No.30923010203), and funding (No.TSXXK2022D002) as well as a startup grant from the NJUST. The authors acknowledge support from the Tianjing Supercomputer Centre, Shanghai Supercomputer Center, and High Performance Computing Platform of Nanjing University of Aeronautics and Astronautics.

---

[1] J. R. Schaibley, H. Yu, G. Clark, P. Rivera, J. S. Ross, K. L. Seyler, W. Yao, and X. Xu, Valleytronics in 2D

materials, Nat. Rev. Mater. **1**, 16055 (2016).

- [2] J. Chu, Y. Wang, X. Wang, K. Hu, G. Rao, C. Gong, C. Wu, H. Hong, X. Wang, K. Liu, C. Gao, and J. Xiong, 2d polarized materials: Ferromagnetic, ferrovalley, ferroelectric materials, and related heterostructures, *Advanced Materials* **33**, 2004469 (2021).
- [3] R. Rong, Y. Liu, X. Nie, W. Zhang, Z. Zhang, Y. Liu, and W. Guo, The interaction of 2d materials with circularly polarized light, *Advanced Science* **10**, 2206191 (2023).
- [4] G. Zhang, H. Wu, W. Jin, L. Yang, B. Xiao, J. Yu, W. Zhang, and H. Chang, Progress and challenges for two-dimensional spin-polarized quantum materials, *Cell Reports Physical Science* **6**, 102356 (2025).
- [5] H. Yu, X. Cui, X. Xu, and W. Yao, Valley excitons in two-dimensional semiconductors, *National Science Review* **2**, 57 (2015).
- [6] P. Rivera, K. L. Seyler, H. Yu, J. R. Schaibley, J. Yan, D. G. Mandrus, W. Yao, and X. Xu, Valley-polarized exciton dynamics in a 2D semiconductor heterostructure, *Science* **351**, 688 (2016).
- [7] K. F. Mak, D. Xiao, and J. Shan, Light–valley interactions in 2D semiconductors, *Nature Photonics* **12**, 451 (2018).
- [8] A. Ciarrocchi, F. Tagarelli, A. Avsar, and A. Kis, Excitonic devices with van der Waals heterostructures: valleytronics meets twistrionics, *Nature Reviews Materials* **7**, 449 (2022).
- [9] R. Xu, Z. Zhang, J. Liang, and H. Zhu, Valleytronics: Fundamental Challenges and Materials Beyond Transition Metal Chalcogenides, *Small*, 2402139 (2024).
- [10] G. Wang, A. Chernikov, M. M. Glazov, T. F. Heinz, X. Marie, T. Amand, and B. Urbaszek, Colloquium: Excitons in atomically thin transition metal dichalcogenides, *Reviews of Modern Physics* **90**, 21001 (2018).
- [11] P. Rivera, H. Yu, K. L. Seyler, N. P. Wilson, W. Yao, and X. Xu, Interlayer valley excitons in heterobilayers of transition metal dichalcogenides, *Nature Nanotechnology* **13**, 1004 (2018).
- [12] Y. Jiang, S. Chen, W. Zheng, B. Zheng, and A. Pan, Interlayer exciton formation, relaxation, and transport in TMD van der Waals heterostructures, *Light: Science & Applications* **10**, 72 (2021).
- [13] M. Selig, F. Katsch, R. Schmidt, S. Michaelis de Vasconcellos, R. Bratschitsch, E. Malic, and A. Knorr, Ultrafast dynamics in monolayer transition metal dichalcogenides: Interplay of dark excitons, phonons, and intervalley exchange, *Physical Review Research* **1**, 022007 (2019), arXiv:1908.10080.
- [14] S. Helmrich, K. Sampson, D. Huang, M. Selig, K. Hao, K. Tran, A. Achstein, C. Young, A. Knorr, E. Malic, U. Woggon, N. Owschimikow, and X. Li, Phonon-Assisted Intervalley Scattering Determines Ultrafast Exciton Dynamics in MoSe<sub>2</sub> Bilayers, *Physical Review Letters* **127**, 157403 (2021), arXiv:2209.08707.
- [15] H.-Y. Chen, D. Sangalli, and M. Bernardi, First-principles ultrafast exciton dynamics and time-domain spectroscopies: Dark-exciton mediated valley depolarization in monolayer WSe<sub>2</sub>, *Physical Review Research* **4**, 043203 (2022), arXiv:2210.05964.
- [16] T. Yu and M. W. Wu, Valley depolarization due to intervalley and intravalley electron-hole exchange interactions in monolayer MoS<sub>2</sub>, *Phys. Rev. B* **89**, 205303 (2014), arXiv:1401.0047.
- [17] M. M. Glazov, E. L. Ivchenko, G. Wang, T. Amand, X. Marie, B. Urbaszek, and B. L. Liu, Spin and valley dynamics of excitons in transition metal dichalcogenide monolayers, *Physica Status Solidi (B) Basic Research* **252**, 2349 (2015), 1504.03911.
- [18] K. S. Thygesen, U. Wurstbauer, B. Miller, E. Parzinger, A. Kormányos, G. Burkard, M. Gmitra, and A. Karamatskou, Spin-flip processes and radiative decay of dark intravalley excitons in transition metal dichalcogenide monolayers, *2D Mater.* **3**, 1 (2016).
- [19] Z. Wang, A. Molina-Sánchez, P. Altmann, D. Sangalli, D. De Fazio, G. Soavi, U. Sassi, F. Bottegoni, F. Ciccacci, M. Finazzi, L. Wirtz, A. C. Ferrari, A. Marini, G. Cerullo, and S. Dal Conte, Intravalley Spin-Flip Relaxation Dynamics in Single-Layer WS<sub>2</sub>, *Nano Lett.* **18**, 6882 (2018).
- [20] L. Guo, M. Wu, T. Cao, D. M. Monahan, Y.-H. Lee, S. G. Louie, and G. R. Fleming, Exchange-driven intravalley mixing of excitons in monolayer transition metal dichalcogenides, *Nature Physics* **15**, 228 (2019).
- [21] S. Xu, C. Si, Y. Li, B. L. Gu, and W. Duan, Valley depolarization dynamics in monolayer transition-metal dichalcogenides: Role of the satellite valley, *Nano Letters* **21**, 1785 (2021).
- [22] X. Jiang, Q. Zheng, Z. Lan, W. A. Saidi, X. Ren, and J. Zhao, Real-time GW -BSE investigations on spin-valley exciton dynamics in monolayer transition metal dichalcogenide, *Science Advances* **7**, eabf3759 (2021).
- [23] Z. Jiang, Y. Li, W. Duan, and S. Zhang, Half-Excitonic Insulator: A Single-Spin Bose-Einstein Condensate, *Phys. Rev. Lett.* **122**, 236402 (2019), arXiv:1811.03738.
- [24] M.-C. Heißenbüttel, T. Deilmann, P. Krüger, and M. Rohlfing, Valley-Dependent Interlayer Excitons in Magnetic WSe<sub>2</sub>/CrI<sub>3</sub>, *Nano Lett.* **21**, 5173 (2021).
- [25] F. Dirnberger, R. Bushati, B. Datta, A. Kumar, A. H. MacDonald, E. Baldini, and V. M. Menon, Spin-correlated exciton–polaritons in a van der Waals magnet, *Nat. Nanotechnol.* **17**, 1060 (2022), arXiv:2203.06129.
- [26] S. Di Sabatino, A. Molina-Sánchez, P. Romaniello, and D. Sangalli, Assignment of excitonic insulators in ab initio theories: The case of NiBr<sub>2</sub>, *Phys. Rev. B* **107**, 115121 (2023), arXiv:2212.11500.
- [27] J. Han, Y. Du, J. Sun, and E. Kan, Magnetic order dependent excitonic effects in monolayer nibr<sub>2</sub>: A first-principles gw+bse study, *Phys. Rev. B* **110**, 115418 (2024).
- [28] M. Wu, Z. Li, T. Cao, and S. G. Louie, Physical origin of giant excitonic and magneto-optical responses in two-dimensional ferromagnetic insulators, *Nat. Commun.* **10**, 2371 (2019).
- [29] L. Zhu and L. Yang, Quasiparticle energies and excitonic effects of chromium trichloride: From two dimensions to bulk, *Phys. Rev. B* **101**, 245401 (2020).
- [30] M. Birowska, P. E. Faria Junior, J. Fabian, and J. Kuntmann, Large exciton binding energies in MnPS<sub>3</sub> as a case study of a van der Waals layered magnet, *Phys. Rev. B* **103**, L121108 (2021).
- [31] A. Molina-Sánchez, G. Catarina, D. Sangalli, and J. Fernández-Rossier, Magneto-optical response of chromium trihalide monolayers: chemical trends, *J. Mater. Chem. C* **8**, 8856 (2020), arXiv:1912.01888.
- [32] M. Wu, Z. Li, and S. G. Louie, Optical and magneto-optical properties of ferromagnetic monolayer CrBr<sub>3</sub>: A first-principles GW and GW plus Bethe-Salpeter equation study, *Phys. Rev. Mater.* **6**, 014008 (2022), arXiv:2106.00770.



- [33] K. L. Seyler, D. Zhong, D. R. Klein, S. Gao, X. Zhang, B. Huang, E. Navarro-Moratalla, L. Yang, D. H. Cobden, M. A. McGuire, W. Yao, D. Xiao, P. Jarillo-Herrero, and X. Xu, Ligand-field helical luminescence in a 2D ferromagnetic insulator, *Nat. Phys.* **14**, 277 (2018), arXiv:1710.05550.
- [34] K. Hwangbo, Q. Zhang, Q. Jiang, Y. Wang, J. Fonseca, C. Wang, G. M. Diederich, D. R. Gamelin, D. Xiao, J. H. Chu, W. Yao, and X. Xu, Highly anisotropic excitons and multiple phonon bound states in a van der Waals antiferromagnetic insulator, *Nat. Nanotechnol.* **16**, 655 (2021), arXiv:2102.10758.
- [35] H.-Y. Ma, M. Hu, N. Li, J. Liu, W. Yao, J.-F. Jia, and J. Liu, Multifunctional antiferromagnetic materials with giant piezomagnetism and noncollinear spin current, *Nat. Commun.* **12**, 2846 (2021).
- [36] Y. Qi, J. Zhao, and H. Zeng, Spin-layer coupling in two-dimensional altermagnetic bilayers with tunable spin and valley splitting properties, *Phys. Rev. B* **110**, 14442 (2024).
- [37] D. Wang, H. Wang, L. Liu, J. Zhang, and H. Zhang, Electric-Field-Induced Switchable Two-Dimensional Altermagnets, *Nano Lett.* **25**, 498 (2025).
- [38] S. Zeng and Y. J. Zhao, Description of two-dimensional altermagnetism: Categorization using spin group theory, *Phys. Rev. B* **110**, 54406 (2024).
- [39] Y. Wu, L. Deng, X. Yin, J. Tong, F. Tian, and X. Zhang, Valley-Related Multipiezo Effect and Noncollinear Spin Current in an Altermagnet Fe 2 Se 2 O Monolayer, *Nano Lett.* **24**, 10534 (2024).
- [40] L. Šmejkal, R. González-Hernández, T. Jungwirth, and J. Sinova, Crystal time-reversal symmetry breaking and spontaneous Hall effect in collinear antiferromagnets, *Science Advances* **6**, eaaz8809 (2020).
- [41] L. Šmejkal, J. Sinova, and T. Jungwirth, Emerging Research Landscape of Altermagnetism, *Phys. Rev. X* **12**, 040501 (2022).
- [42] Y.-P. Zhu, X. Chen, X.-R. Liu, Y. Liu, P. Liu, H. Zha, G. Qu, C. Hong, J. Li, Z. Jiang, X.-M. Ma, Y.-J. Hao, M.-Y. Zhu, W. Liu, M. Zeng, S. Jayaram, M. Lenger, J. Ding, S. Mo, K. Tanaka, M. Arita, Z. Liu, M. Ye, D. Shen, J. Wrachtrup, Y. Huang, R.-H. He, S. Qiao, Q. Liu, and C. Liu, Observation of plaid-like spin splitting in a noncoplanar antiferromagnet, *Nature* **626**, 523 (2024).
- [43] J. Krempaský, L. Šmejkal, S. W. D'Souza, M. Hajlaoui, G. Springholz, K. Uhlířová, F. Alarab, P. C. Constantinou, V. Strocov, D. Usanov, W. R. Pudenko, R. González-Hernández, A. Birk Hellenes, Z. Jansa, H. Reichlová, Z. Šobán, R. D. Gonzalez Betancourt, P. Wadley, J. Sinova, D. Kriegner, J. Minár, J. H. Dil, and T. Jungwirth, Altermagnetic lifting of Kramers spin degeneracy, *Nature* **626**, 517 (2024).
- [44] C. Song, H. Bai, Z. Zhou, L. Han, H. Reichlova, J. H. Dil, J. Liu, X. Chen, and F. Pan, Altermagnets as a new class of functional materials, *Nature Reviews Materials* 10.1038/s41578-025-00779-1 (2025).
- [45] Z. M. Yu, S. Guan, X. L. Sheng, W. Gao, and S. A. Yang, Valley-Layer Coupling: A New Design Principle for Valleytronics, *Phys. Rev. Lett.* **124**, 37701 (2020), arXiv:1904.06498.
- [46] R.-W. Zhang, C. Cui, R. Li, J. Duan, L. Li, Z.-M. Yu, and Y. Yao, Predictable Gate-Field Control of Spin in Altermagnets with Spin-Layer Coupling, *Phys. Rev. Lett.* **133**, 056401 (2024), arXiv:2306.08902.
- [47] P. Giannozzi, S. Baroni, N. Bonini, M. Calandra, R. Car, C. Cavazzoni, D. Ceresoli, G. L. Chiarotti, M. Cococcioni, I. Dabo, A. Dal Corso, S. de Gironcoli, S. Fabris, G. Fratesi, R. Gebauer, U. Gerstmann, C. Gougoussis, A. Kokalj, M. Lazzeri, L. Martin-Samos, N. Marzari, F. Mauri, R. Mazzarello, S. Paolini, A. Pasquarello, L. Paulatto, C. Sbraccia, S. Scandolo, G. Sclauzero, A. P. Seitsonen, A. Smogunov, P. Umari, and R. M. Wentzcovitch, Quantum espresso: a modular and open-source software project for quantum simulations of materials, *J. Phys. Condens. Matter* **21**, 395502 (2009).
- [48] D. R. Hamann, Optimized norm-conserving vanderbilt pseudopotentials, *Phys. Rev. B* **88**, 085117 (2013).
- [49] M. van Setten, M. Giantomassi, E. Bousquet, M. Verstraete, D. Hamann, X. Gonze, and G.-M. Rignanese, The pseudodojo: Training and grading a 85 element optimized norm-conserving pseudopotential table, *Computer Physics Communications* **226**, 39 (2018).
- [50] J. P. Perdew, K. Burke, and M. Ernzerhof, Generalized gradient approximation made simple, *Phys. Rev. Lett.* **77**, 3865 (1996).
- [51] H. Lin, J. Si, X. Zhu, K. Cai, H. Li, L. Kong, X. Yu, and H.-H. Wen, Structure and physical properties of  $\text{csv}_2\text{se}_{2-x}\text{o}$  and  $\text{v}_2\text{se}_2\text{o}$ , *Phys. Rev. B* **98**, 075132 (2018).
- [52] T. e. a. Ozaki, Openmx (open source package for material explorer), <http://www.openmx-square.org>; T. Ozaki, Variationally optimized atomic orbitals for large-scale electronic structures, *Phys. Rev. B* **67**, 155108 (2003); T. Ozaki and H. Kino, Numerical atomic basis orbitals from h to kr, *ibid.* **69**, 195113 (2004); Efficient projector expansion for the ab initio lcao method, **72**, 045121 (2005); X. He, N. Helbig, M. J. Verstraete, and E. Bousquet, Tb2j: A python package for computing magnetic interaction parameters, *Comput. Phys. Commun.* **264**, 107938 (2021); H. Yoon, T. Kim, J.-H. Sim, and M. Han, An open-source software for calculating magnetic interactions based on magnetic force theory, **247**, 106927 (2020); L. Liu, X. Ren, J. Xie, B. Cheng, W. Liu, T. An, H. Qin, and J. Hu, Magnetic switches via electric field in bn nanoribbons, *Appl. Surf. Sci.* **480**, 300 (2019).
- [53] C. Adamo and V. Barone, Toward reliable density functional methods without adjustable parameters: The pbe0 model, *The Journal of Chemical Physics* **110**, 6158 (1999).
- [54] J. Heyd, G. E. Scuseria, and M. Ernzerhof, Erratum: "hybrid functionals based on a screened coulomb potential" [*j. chem. phys.* 118, 8207 (2003)], *The Journal of Chemical Physics* **124**, 219906 (2006).
- [55] H. Jiang, R. I. Gomez-Abal, P. Rinke, and M. Scheffler, First-principles modeling of localized *d* states with the *gw*@LDA + *u* approach, *Physical Review B* **82**, 045108 (2010).
- [56] See Supplemental Material at <http://...> for the following details: (1) Methodology dependent ground state. (2) Convergence tests for GW. (3) Choice of scissor operator. (4) Magnetic properties of monolayer  $\text{V}_2\text{X}_2\text{O}$  ( $X = \text{S}, \text{Se}, \text{Te}$ ). (5) Results for monolayer  $\text{V}_2\text{Se}_2\text{O}$ . (6) Results for other interlayer excitons in AB-stacking.
- [57] J.-L. Li, G.-M. Rignanese, E. K. Chang, X. Blase, and S. G. Louie, GW study of the metal-insulator transition of bcc hydrogen, *Phys. Rev. B* **66**, 035102 (2002).
- [58] M. S. Hybertsen and S. G. Louie, Electron correlation in semiconductors and insulators: Band gaps and quasipar-

- ticle energies, Phys. Rev. B **34**, 5390 (1986).
- [59] R. W. Godby and R. J. Needs, Metal-insulator transition in kohn-sham theory and quasiparticle theory, Phys. Rev. Lett. **62**, 1169 (1989).
  - [60] M. Rohlfing and S. G. Louie, Electron-hole excitations and optical spectra from first principles, Phys. Rev. B **62**, 4927 (2000).
  - [61] L. X. Benedict and E. L. Shirley, Ab initio calculation of  $\epsilon_2(\omega)$  including the electron-hole interaction: Application to gan and  $\text{caf}_2$ , Phys. Rev. B **59**, 5441 (1999).
  - [62] S. Ismail-Beigi, Truncation of periodic image interactions for confined systems, Phys. Rev. B **73**, 233103 (2006).
  - [63] J. Deslippe, G. Samsonidze, D. A. Strubbe, M. Jain, M. L. Cohen, and S. G. Louie, Berkeleygw: A massively parallel computer package for the calculation of the quasiparticle and optical properties of materials and nanostructures, Comput. Phys. Commun. **183**, 1269 (2012).
  - [64] M. Palummo, M. Bernardi, and J. C. Grossman, Exciton Radiative Lifetimes in Two-Dimensional Transition Metal Dichalcogenides, Nano Letters **15**, 2794 (2015).
  - [65] H.-Y. Chen, V. A. Jhalani, M. Palummo, and M. Bernardi, Ab Initio Calculations of Exciton Radiative Lifetimes in Bulk Crystals, Nanostructures and Molecules, Physical Review B **100**, 75135 (2019), arXiv:1901.08747.